JGR Solid Earth

RESEARCH ARTICLE
10.1029/2020JB021350

A High-Resolution Paleosecular Variation Record for Marine Isotope Stage 6 From Southeastern Black Sea Sediments

Norbert R. Nowaczyk[1], Jiabo Liu[1,2], Birgit Plessen[1], Antje Wegwerth[3], and Helge W. Arz[3]

[1]Helmholtz Centre Potsdam, GFZ German Research Centre for Geosciences, Section Paleoclimate and Landscape Evolution, Potsdam, Germany, [2]Department of Ocean Science and Engineering, Southern University of Science and Technology, Shenzhen, China, [3]Leibniz Institute for Baltic Sea Research Warnemünde, Rostock, Germany

Key Points:

- Reconstructed geomagnetic field variation record between 180 and 130 ka from Black Sea sediments
- First full-vector paleosecular variation record from marine isotope stage 6 for Southeast Europe/Southwest Asia
- Intensity maxima occur at 166.5 ka and at 141.0 ka

Supporting Information:

- Supporting Information S1

Correspondence to:

N. R. Nowaczyk,
norbert.nowaczyk@gfz-potsdam.de

Citation:

Nowaczyk, N. R., Liu, J., Plessen, B., Wegwerth, A., & Arz, H. W. (2021). A high-resolution paleosecular variation record for marine isotope stage 6 from Southeastern Black Sea sediments. *Journal of Geophysical Research: Solid Earth*, *126*, e2020JB021350. https://doi.org/10.1029/2020JB021350

Received 12 NOV 2020
Accepted 4 FEB 2021

Abstract A full-vector paleosecular variation (PSV) record (inclination, declination, and relative paleointensity) from the pen-ultimate glacial (130–180 ka) could be constructed from a total of 12 sediment cores recovered from the Arkhangelsky Ridge in the SE Black Sea. Stacking of the individual partly fragmented records was achieved by a detailed correlation using high-resolution data records from X-ray fluorescence scanning, Ca/Ti and K/Ti log-ratios, as well as magnetic susceptibility. Age constraints are provided by a detailed composite oxygen isotope stratigraphy from three of the cores, correlated to U-Th-dated speleothem oxygen isotope records from Hungary and Turkey. The temporal resolution of the stacked paleomagnetic data records is 200 years. Practically, this data set is the first high-resolution PSV record for SE Europe/SW Asia from marine isotope stage 6, comprising inclination, declination and relative paleointensity. Besides an easterly swing in declination at ~159 ka and a pronounced intensity low together with low inclinations at ~148 ka, both not reaching an excursional PSV index of >0.5, the obtained directional variations reflect only normal PSVs, with a PSV index of <0.3.

1. Introduction

Studying the geometry and dynamics of the Earth's magnetic field in time in the very detail requires the acquisition of long continuous well-dated high-quality and high-resolution paleosecular variation (PSV) records from all over the globe. Such records, theoretically, should be obtainable from any sedimentary sequence, either marine or lacustrine, that was deposited with high sedimentation rates. However, this is the case only for certain lakes and restricted areas of the world's oceans that are close to the shore with a high input of lithogenic material from the continents by rivers/and or glaciers. Thus, for example, magneto-stratigraphic records obtained from the largest ocean, the Pacific Ocean, are often characterized only by low resolution (1,000 years, e.g., Yamazaki & Ioka, 1994; Yamazaki et al., 2008) but reaching far back in time, for example, back to 10 Ma (Yamazaki & Yamamoto, 2018), with sedimentation rates of just some 1–2 cm ka^{-1}. On the other hand, sites closer to the shore such as ODP Site 1233 in the SE Pacific, offshore Chile, can reach sedimentation rates as high as ~175 cm ka^{-1} (Lund et al., 2006), providing an extremely high-resolution paleomagnetic record, but only for the past about 70 ka.

A common problem, for paleomagnetism, is that lake sediments often contain high percentages of organic matter. Such (layers of) sediments are generally associated with very low intensities and may also carry only unstable magnetizations. The presence of organic matter also frequently causes early diagenetic dissolution of magnetite and the precipitation of greigite (Fe_3S_4; Skinner et al., 1964) such as in Lake Baikal, Russia (e.g., Demory et al., 2005) or in Lake Ohrid, Macedonia/Albania (Just et al., 2016), corrupting the directional and/or paleointensity record to a large degree. Besides marine and lacustrine archives, paleomagnetic data for reconstructions of the Earth magnetic field are also generated through archeomagnetic investigations, which are mostly restricted to the Holocene (e.g., Korte & Constable, 2011; Korte et al., 2011). With the availability of an increasing number of high-resolution data preceding the Holocene (e.g., Liu et al., 2020; Lund, 2018) first field models going back in time to 100 ka could be developed recently (e.g., Korte et al., 2019; Panovska et al., 2019).

This study is part of a comprehensive multidisciplinary investigation on a total of 18 sediment cores recovered during two ship expeditions from the Arkhangelsky Ridge in the SE Black Sea (Figure 1). Some of the

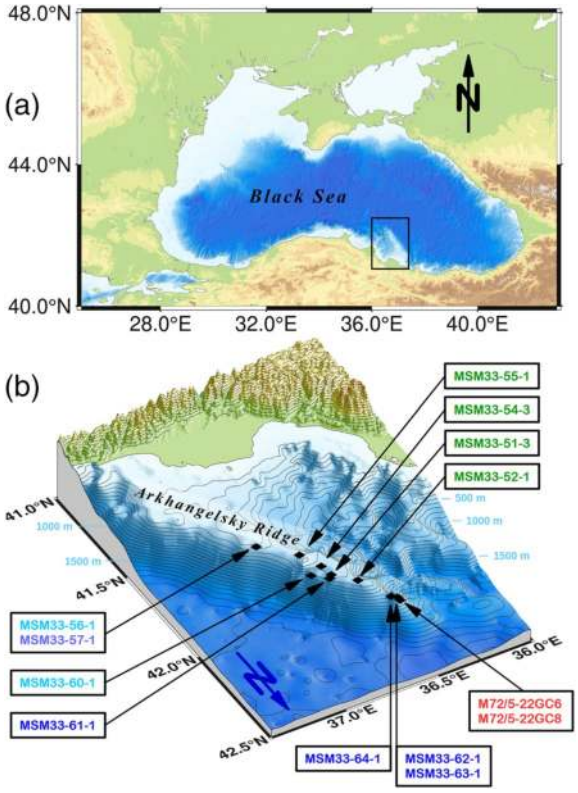

Figure 1. Position of the study area in (a) the Black Sea, with (b) coring sites along the Arkhangelsky Ridge (black rectangle in a). Bathymetric contour lines are shown every 100 m. For reasons of clarity core numbers (and related data presented in further Figures) are shown in different colors. Red indicates cores from RV Meteor expedition M72/5 in 2007, while green and blue refer to cores from RV Maria S. Merian expedition MSM33 in 2013. Lighter hues of blue indicate the cores providing the age model for this study (MSM33-56-1, 57-1, 60-1).

cores cover a time window back to about 180 ka, but with a major erosive hiatus from about 68 to 125 ka. Paleoenvironmental investigations were conducted by Shumilovskikh et al. (2012, 2013a, 2013b, 2014). Geochemical analyses and paleoclimatic studies on the cores were published by Wegwerth et al. (2014, 2015, 2016, 2018, 2019, 2020). Chronological and geochemical data on tephras found in the sediments is provided by Nowaczyk et al. (2012), Cullen et al. (2014), and Wegwerth et al. (2019). Czymzik et al. (2020) performed a first investigation of the cosmogenic radioisotope 10Be in Black sea sediments during Greenland-interstadial 10. Paleo- and rock magnetic investigations focusing on sediments from the last glacial, marine isotope stages (MIS) 2–4 were published by Nowaczyk (2020), Nowaczyk et al. (2012, 2013, 2018, 2021a) and Liu et al. (2018, 2019, 2020). Here we present the final paleo- and rock magnetic study summarizing data from the pen-ultimate glacial, MIS 6, providing a high-resolution full-vector PSV curve (inclination, declination, and relative paleointensity) from 130 ka back to 180 ka, based on 12 of the 18 cores from the Arkhangelsky Ridge, SE Black Sea.

2. Materials and Methods

2.1. Sediment Composition

During two ship expeditions to the SE Black Sea a total of 18 cores were recovered from the Arkhangelsky Ridge, with six cores taken by German RV Meteor in 2007 (leg M72/5), and 12 cores taken by German RV Maria S. Merian in 2013 (leg MSM33). Thirteen of these cores (Table 1, Figure 1) provide sediments that were deposited during the penultimate glacial (MIS 6) at fairly high sedimentation rates. Similar to the last glacial, MIS 2 to 4, MIS 6 sediments consist mostly of homogeneous fine grained organic-poor brownish to greyish silici-clastic mud with variable amounts of calcium carbonate and abundant coastal ice rafted detritus (IRD), Such deposits indicate the formation of coastal winter ice along the southern Black Sea margin during cold periods of the last glacials (Nowaczyk et al., 2012). Downcore X-ray fluorescence (XRF) scanning of MSM33 cores was performed at the Leibniz Institute for Baltic Sea Research Warnemünde, Rostock, Germany using a COX Analytics ITRAX XRF Core Scanner. It was operated with a Cr-tube at 30 kV and 30 mA and a SDD Si drift detector. Exposure time was 15 s at a step size of 1 mm. Data obtained from this method was mainly used for correlation purposes. MIS 6 sediments do not show clear traces of bioturbation, though deposited mostly under freshwater lacustrine conditions. Frequently abundant ostracods, therefore, could be used for a detailed oxygen isotope stratigraphy (see Section 2.2). Three tephra layers could also be identified in MIS 6 sediments. These detailed analyses of the MIS 6 sediments and their chronology are provided by Wegwerth et al. (2014, 2019). Overlying (lower) Eemian (MIS 5e) sediments are built up of soft laminated dark green organic-rich marine sapropels and layers of whitish coccolith oozes. These anoxic sediments are unsuitable for paleomagnetic investigation due to their low intensity and frequently occurring greigite. Like in MIS 2 to 4 sediments, greigite is also present in MIS 6 sediments, mostly occurring sporadically and concentrated in nonstratiform nodules in some rare cases of up to 2 cm. Some of these nodules partly consist of pure greigite, as tested by scanning electron microscopy and energy dispersive X-ray spectroscopy (EDS). It also resides concentrated in the pore spaces of the tephras (unpublished data).

2.2. Oxygen Isotope Stratigraphy

For a paleoclimatic investigation of MIS 6 in the SE Black Sea a detailed oxygen isotope ($\delta^{18}O$) stratigraphy, based on ostracods (>150 μm) picked from core MSM33-60-1, was elaborated. The record was supplement-

Table 1
List of Cores and Publications with Further Detailed Paleo- and Rock Magnetic Data Relevant for this Study

Core number	Length (cm)	Water depth (m)	Latitude	Longitude	Publication
MSM33-55-1 PC	948	362.4	41° 54.01' N	36° 46.98' E	Liu et al. (2019)
MSM33-56-1	736	373.9	41° 47.33' N	36° 55.81' E	This study
MSM33-57-1	778	374.0	41° 47.38' N	36° 55.95' E	Liu et al. (2018, 2019)
MSM33-54-3 PC	953	382.2	41° 58.99' N	36° 43.85' E	Nowaczyk et al. (2018)
MSM33-51-3 PC	1,027	428.4	42° 02.38' N	36° 43.08' E	Nowaczyk et al. (2018)
MSM33-52-1	682	467.4	41° 05.08' N	36° 37.19' E	this study
MSM33-61-1	746	479.3	42° 02.85' N	36° 44.02' E	Liu et al. (2019)
MSM33-60-1	739	498.	41° 58.62' N	36° 47.53' E	this study
MSM33-64-1	721	660.5	42° 12.46' N	36° 31.52' E	Nowaczyk et al. (2018)
MSM33-62-1	747	767.3	42° 13.15' N	36° 30.11' E	Liu et al. (2018)
MSM33-63-1	704	785.5	42° 13.27' N	36° 30.00' E	Liu et al. (2018)
M72/5-22GC6	800	842.6	42° 13.57' N	36° 29.65' E	Nowaczyk et al. (2012, 2013)
M72/5-22GC8	945	847.0	42° 13.53' N	36° 29.59' E	Nowaczyk et al. (2012, 2013)

Notes. Colors are used to group the set of cores. Red indicates cores from RV Meteor expedition M72/5 in 2007, while green and blue refer to cores from RV Maria S. Merian expedition MSM33 in 2013. Lighter hues of blue indicate the cores providing the age model for this study (MSM33-56-1, 57-1, 60-1).

ed with data from cores MSM33-56-1 and MSM33-57-1 (Figure 1, Table 1) which extend further back in time. Thus, the $\delta^{18}O$ composite record covers the time interval from 127 ka back to about 184 ka. More details are provided by Wegwerth et al. (2019).

2.3. Paleo- and Mineral Magnetism

Continuous high-resolution logging of magnetic susceptibility was accomplished using a Bartington MS2E/1 spot-reading sensor integrated into an automatic logging system. Measurements were performed on split cores in steps of 1 mm with determination of the sensor's drift every 10 mm by readings in air. The response function of the sensor with respect to a thin magnetic layer is a Gaussian curve with half-width of slightly less than 4 mm.

The split cores were then sampled along their central axes using clear cubic plastic boxes of 20 × 20 × 15 mm internal size. The 6 cm^3 big boxes were pressed into the sediment either with their edges parallel to the cores' axes (sample distance 23–30 mm), or in two parallel rows with the boxes' diagonals parallel to the cores' axes (rotated by 45°), with an offset of half a box between the two rows (sample distance 16–17 mm). This special sampling technique was invented by Nowaczyk et al. (2012), with a detailed illustration provided by Nowaczyk et al. (2021a).

An AGICO Multifunction Kappabridge MFK1-A was used to determine the anisotropy of magnetic susceptibility (AMS) for most of the samples. The AGICO software provided also the bulk (low field) susceptibility κ_{LF} as well as the orientations and normalized lengths of the principal anisotropy axes K_{max}, K_{int}, and K_{min}. The degree of anisotropy was calculated as:

$$\text{degree}(\text{AMS}) = 100 \times (K_{max} - K_{min}) / K_{max} \quad (1)$$

given in per cent. The shape of the AMS ellipsoid defined by the principal axes was calculated as:

$$\text{shape}(\text{AMS}) = (K_{max} \times K_{min}) / K_{int}^2 \quad (2)$$

with shape (AMS) < 1 (>1) for an oblate (prolate) magnetic fabric. For an undisturbed sedimentary fabric shape(AMS) is <1 and the minimum axis K_{min} is oriented perpendicular to the bedding plane (inclina-

tion(K_{min}) ~90°). High-temperature measurements of magnetic susceptibility up to 700°C in Argon atmosphere were also performed by using the MFK1-A in combination with a CS-3 unit.

The natural remanent magnetization (NRM) of the samples were measured with an automated 2G Enterprises 755 cryogenic long-core magnetometer with an in-line tri-axial alternating field (AF) demagnetizer. All paleomagnetic samples were stepwise AF demagnetized in 11 steps with peak amplitudes of 0, 5, 10, 15, 20, 30, 40, 50, 65, 80, and 100 mT. AF demagnetization results were subjected to principal component analysis according to Kirschvink (1980) in order to determine the direction of the characteristic remanent magnetization (ChRM). During expedition MSM33, the majority of the cores was recovered from along the slopes of the Arkhangelsky Ridge (Figure 1). Here, the subbottom profiling system aboard RV Maria S. Merian partly indicated tectonically tilted but intact sediment sequences at several coring sites. Therefore, in cases where abnormal ChRM inclinations were observed, assuming an intact and only tilted magnetic/sedimentary fabric, the tilt angle and tilt direction of K_{min} was used to correct paleomagnetic directions. Further on, the positions of the virtual geomagnetic poles (VGPs) were calculated from the ChRM directions.

Anhysteretic remanent magnetizations (ARM) were imparted with an AF peak amplitude of 100 mT superimposed by a 50 μT static field using a separate 2G Enterprises 600 single-axis AF demagnetizer. ARMs then were measured and AF demagnetized (0, 10, 20, 30, 40, 50, 65, 80 mT) using the long-core magnetometer system in order to provide the data basis for the estimation of relative paleointensity by determining the slope of NRM versus ARM intensity of common demagnetization steps using linear regression. Since the Black Sea MIS 6 sediments have mineral magnetic properties similar to the MIS 2 to 4 sediments, relative paleointensities were then converted into virtual axial dipole moments (VADM) by using a conversion factor of 14.52×10^{22} Am^2, empirically determined from the comparison of relative paleointensities obtained from MIS 2 to 4 sediments to absolute paleointensities of the same time interval (Nowaczyk et al., 2013). In order to quantify the obtained paleomagnetic information (ChRM directions, VGP positions, relative paleointensity) the PSV index was calculated according to Panovska and Constable (2017):

$$PSV\ \text{index} = M_0\ /\ VADM \times \left(\pi\ /\ 2 - \lambda_{VGP}\right) / \pi \tag{3}$$

with M_0 being the present day magnetic moment of the Earth (8.0×10^{22} Am^2) and λ_{VGP} being the VGP latitude in radian.

Saturated isothermal remanent magnetizations (SIRM) were imparted with a static field of 1.5 T using a 2G Enterprises 660 pulse magnetizer. In order to determine the S-ratio a reversed field of 0.2 T was applied:

$$S - \text{ratio} = 0.5 \times \left(1 - \left[IRM\left(-0.2T\right) / SIRM\left(1.5T\right)\right]\right). \tag{4}$$

A field of 0.2 T was chosen by lab experience in order to optimally separate the contributions from high-coercive hematite (Fe_2O_3), with S-ratios close to 0, and low-coercive magnetite (Fe_3O_4) and greigite (Fe_3S_4), with S-ratios approaching 1. IRMs were measured with a Molyneux spinner magnetometer, since acquired IRMs (up to 2,800 Am^{-1}) would have massively overranged the cryogenic magnetometer. In order to distinguish greigite from magnetite the SIRM/k_{LF} ratio was determined, with values below 10 kAm^{-1} indicating samples that are dominated by magnetite while values above indicate an increasing significant contribution of greigite (Nowaczyk et al., 2012, 2013). SIRM/k_{LF} ratios reaching 50 to 100 kAm^{-1} were found to indicate that greigite is the dominating magnetic mineral in a sample.

Measurements of IRM acquisition curves and first order reversal curves (FORCs) diagrams were performed on a 4" Princeton Measurements Corporation "MicroMag 2900" alternating gradient magnetometer (AGM) using about 20 mg small subsamples. IRM acquisition curves were measured on logarithmically spaced field steps from 2 mT to 1 T. The obtained IRM acquisition curves were further decomposed into different coercivity components using the software "pyIRM" (https://github.com/botaoxiongyong/pyIRM). The protocol and calculation of irregular FORC (irFORC) and transient hysteresis FORC (tFORC) diagrams were performed following Zhao et al. (2017). More detailed descriptions of applied paleo- and mineral magnetic methods are provided by Liu et al. (2018, 2019, 2020) and Nowaczyk et al. (2012, 2013, 2018, 2020).

3. Results

3.1. Oxygen Isotope Stratigraphy and Age Models

Dating of MIS 6 sediments from the Arkhangelsky Ridge is mainly based on the $\delta^{18}O$ composite record (MSM33-60-1/56-1/57-1) provided by Wegwerth et al. (2019). To derive depth age tie points it was correlated to $^{234}U/^{230}Th$ dated $\delta^{18}O$ speleothem records from Sofular Cave (Anatolia; Badertscher et al., 2011) and Abaliget Cave (Hungary; Koltai et al., 2017). Further age tie points were provided by three tephra layers with ages of 130.9 ± 0.7 ka, 161 ± 2 ka, and 167 ± 1 ka (Wegwerth et al., 2019, and references therein), identified in cores MSM33-60-1 and MSM33-61-1 (Figure 1). All other cores presented in this study were then correlated to the composite, using results from high-resolution XRF-scanning, mainly Ca/Ti and K/Ti log-ratios, magnetic susceptibility logging, as well as by using their paleo- and rock magnetic results. Individual records and a stack of Ca/Ti (K/Ti) log-ratios, together with the $\delta^{18}O$ data from MIS 6 sediments are shown in Figure 2 (Figure S1). The temporal positions of the tephra layers are indicated by three brown triangles in Figure 2 (Figures S1 and S2). The final age models for all cores discussed in this paper are shown in Figure 3. Sedimentation rates range from ~5 to ~20 $cmka^{-1}$ in most of MIS 6, with maximum values of up to 40 $cmka^{-1}$ approaching Termination II (MIS 6/5 boundary). Due to the fact that the cores were recovered from the slope of the tectonically active Arkhangelsky Ridge several hiatuses of different duration were detected in various cores. Actually, these sites were explicitly chosen from subbottom profiling data in order to gain access to older sediments by coring with gravity and piston corers with barrel lengths of only 12 m (Arz et al., 2014).

3.2. Paleo- and Mineral Magnetic Results

All investigated samples from MIS 6 are characterized by more or less steep positive inclinations resembling typical secular variation patterns according to the site latitude of 42°N. Vector endpoint diagrams of typical demagnetization results from core MSM33-60-1 are shown in Figure 4. Only two different types of behavior for MIS 6 sediments were observed. Vector endpoints of magnetite-dominated samples ($SIRM/k_{LF} \leq 10$ kAm^{-1}) migrate straight toward the origin, partly with some minor viscous components visible during the first demagnetization steps, partly with some slight overshoot across the origin at the final demagnetization steps. However, this occurs at NRM levels of clearly less than 10% (Figures 4a, 4c and 4e). In general, six to eight successive demagnetization steps could be used for ChRM determination (dark blue and dark red symbols in Figure 4). In contrast to this, greigite-dominated samples ($SIRM/k_{LF} >> 10$ kAm^{-1}) exhibit partly a massive acquisition of a gyro-remanent magnetization (GRM) during AF demagnetization, starting at an AF level of 50 mT, with vector endpoints passing by the origin (Figures 4d and 4f). For such samples only AF steps lying on a straight line pointing toward the origin were used tentatively for ChRM determination (see also Nowaczyk et al., 2020a). Note that greigite-dominated samples (Figures 4d and 4f) have NRMs about 50 times higher than magnetite-dominated samples.

Some rock magnetic results from samples from core MSM33-60-1 that were used for creation of the paleomagnetic stacks (with $SIRM/\kappa_{LF} < 10$ kAm^{-1}) are shown in Figure 5. . In high-temperature magnetic susceptibility κ_{LF} curves (Figure 5a), the unique Curie-temperature of about 580°C indicates the dominance of low-Ti magnetite in all samples. The cooling curves show a three- to five-fold increase in susceptibility, indicating the new formation of magnetite. The decomposition of IRM acquisition curves can provide information about coercivity distributions of different mineral assemblages in natural samples (Heslop et al., 2004). For all studied samples, three IRM components can be identified (Figure 5b). Specifically, the dominant IRM component with a median field of about 34–40 mT contributes to more than 75% of the total IRM. The irFORC and tFORC diagrams were performed on irregularly spaced field grids and calculated with a smooth factor of 3. In all samples, their irFORC distributions spread along the B_i axis up to about ~70 mT. This pattern is typical for "pseudo-single domain," or "vortex state" materials (e.g., Roberts et al., 2014; Zhao et al., 2017). In addition, distributions of tFORC exhibit two peaks above and below the $B_i = 0$ axis, respectively (Figure 5d). The symmetric pattern of tFORC likely implies the existence of noninteracting stable single domain particles (e.g., Zhao et al., 2017).

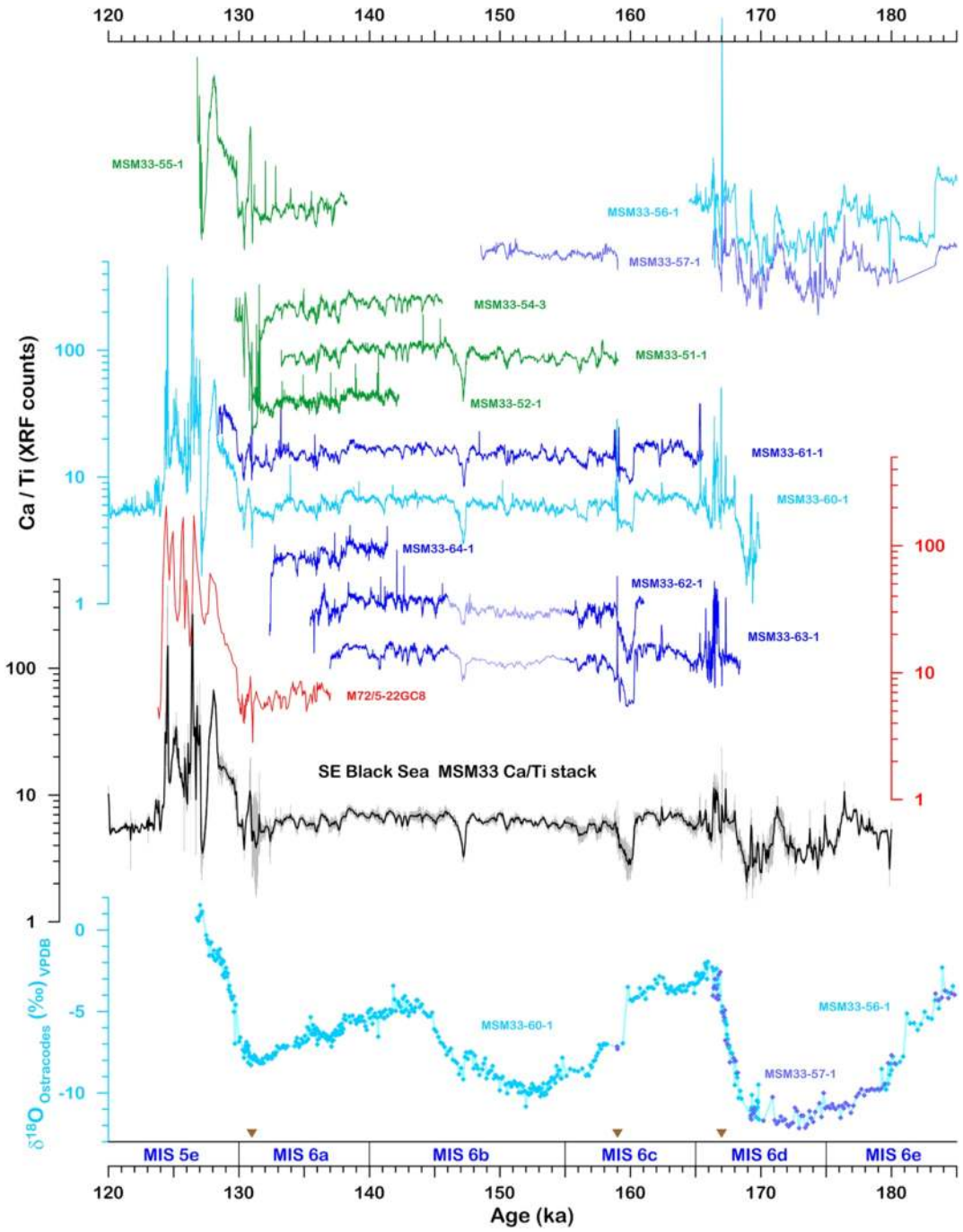

Figure 2. Paleoclimatic data from MIS 6 sediments from the SE Black Sea shown as individual records of XRF-derived Ca/Ti log-ratios from each core used for this study and stacked Ca/Ti log-ratios, together with the $\delta^{18}O$ composite record from MIS 6 sediments (Wegwerth et al., 2019) based on cores MSM33-60-1, MSM33-56-1, and MSM33-57-1. The individual Ca/Ti ratios are shown with a constant offset from core to core, with some *y*-axes shown in the same color as the corresponding core/stack data. Brown triangles in the bottom indicate the chronological positions of three tephra layers identified in several cores. The light blue sections in the records from cores MSM33-62-1 and 63-1 indicate questionable core intervals which seem to be disturbed. They were not used for stacking.

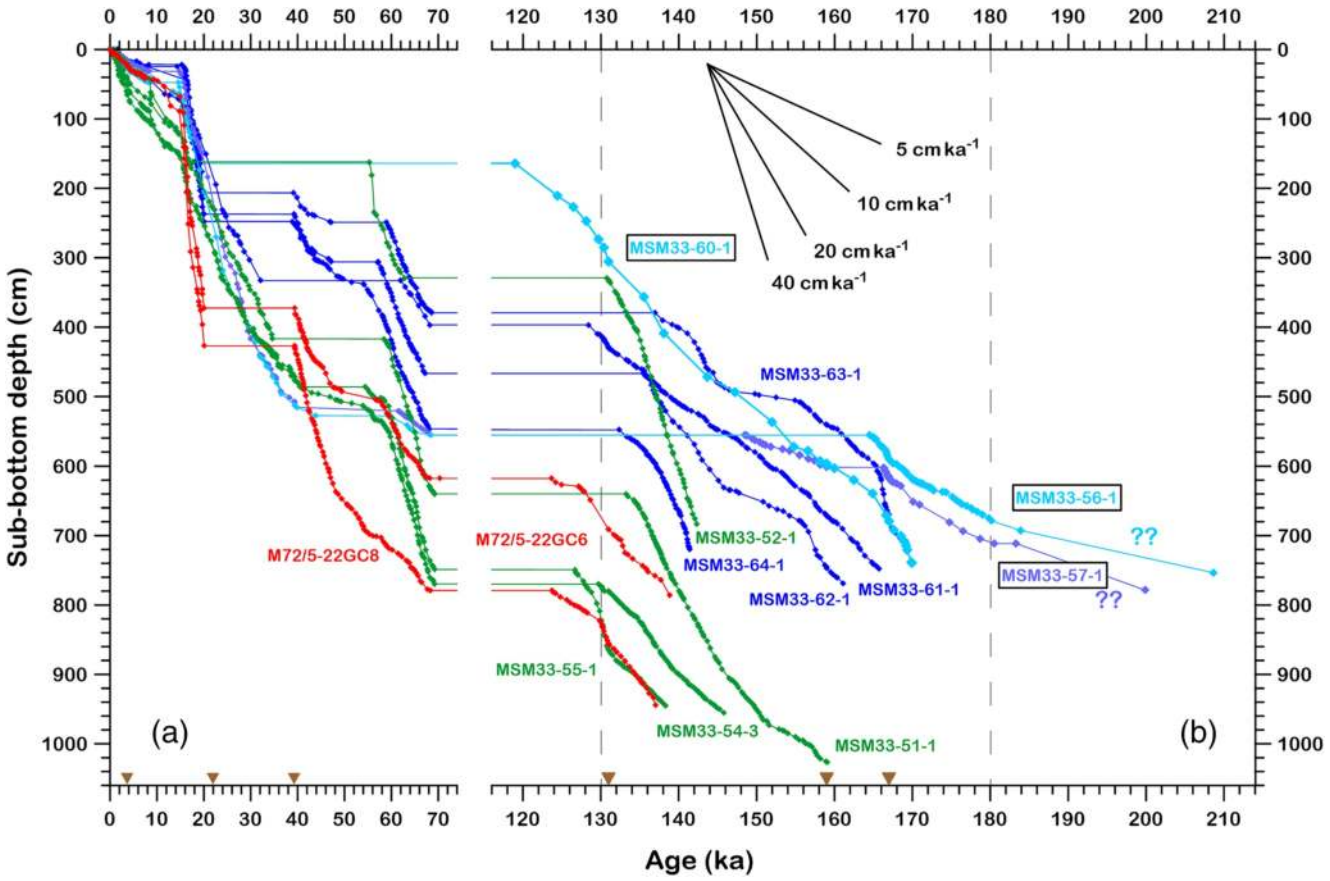

Figure 3. Final age models for all cores from the SE Black Sea consulted for this study (see also Figure 1), with focus on MIS 6. Brown triangles in the bottom indicate the chronological positions of three tephra layers in the Holocene and the last glacial, respectively (Cullen et al., 2014), and three tephra layers in MIS 6 as discussed by Wegwerth et al. (2019). The various, partly long hiatuses are due to the tectonic activity of the study area and associated slumping of sediment packages triggered by earthquakes. The slopes of the black lines in the upper right represent the range of sedimentation rates of the studied sediments (MIS 6 only). Black frames indicate the cores providing the age model for MIS 6 sediments from all investigated sites. Vertical dashed gray lines mark the time interval from which paleomagnetic data was used for stacking.

Figure 6 shows downcore variations of ChRM inclination and declination, relative paleointensity (slope (NRM/ARM)), S-ratio and the SIRM/κ_{LF} ratio from cores MSM33-52-1, MSM33-56-1, and MSM33-60-1. Similar results were previously published for all other cores used for this paper, according to Table 1. AMS analyses (Figures S3–S6) revealed that some sections of the sedimentary sequences are characterized by a magnetic fabric with a significantly tilted small principal axis K_{min}, normally oriented vertically in an undistorted sedimentary magnetic fabric. Often such anomalous fabrics are associated with anomalous paleomagnetic directions, such as in core MSM33-60-1 between 500 and 600 cm (orange curves in Figure 6c), with inclinations being too shallow. Therefore, paleomagnetic directions were corrected according to the direction and amount of tilt of the K_{min} axis, thus resulting in steeper inclinations oscillating around the inclination of a geocentric axial dipole at 42°N (61°; vertical green dashed lines). As in the previous studies (e.g., Nowaczyk et al. 2012; Liu et al., 2018), samples with SIRM/κ_{LF} > 10 kAm^{-1}, found to be contaminated by greigite, were not consulted for further paleomagnetic interpretations. Lastly, paleomagnetic directions were rotated so that a mean declination of 0° was obtained for MIS 6 sediments. The final records of ChRM directions and relative paleointensity are shown as black curves in Figure 6. Core MSM33-52-1 (Figure 6a) provides the highest resolution of late MIS 6 with the lowermost 3.5 m representing just the time interval from 131 back to 142 ka (see Figure 3). Core MSM33-56-1 (Figure 6b), together with MSM33-57-1 (Liu et al., 2018, 2019), reach back to at least 185 ka with some older sediments of unknown age (Wegwerth et al., 2019; Figure 3). Core MSM33-60-1 (Figure 6c), sampled at high resolution from 249 cm onward, together with cores MSM33-61-1 (Liu et al., 2019) and MSM33-51-1 (Nowaczyk et al., 2018) cover most of MIS

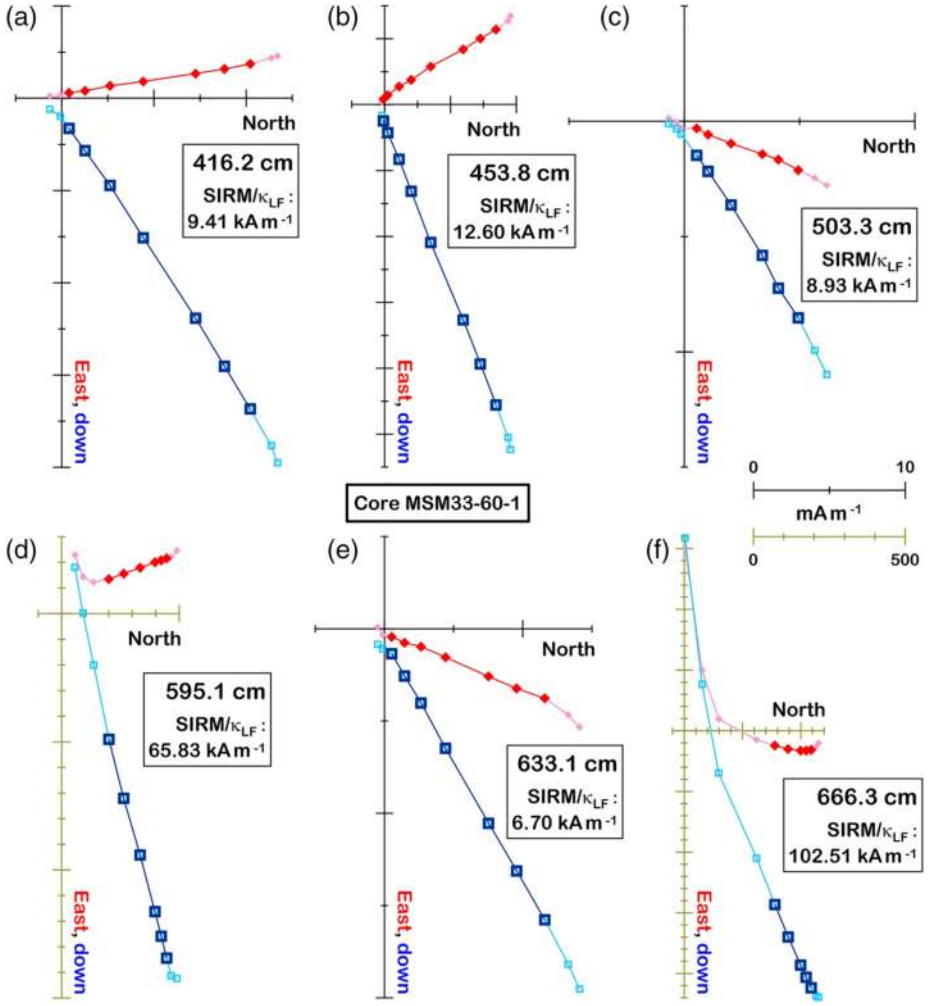

Figure 4. Vector endpoint diagrams of alternating field (AF) demagnetization results from six selected samples from core MSM33-60-1. Pink/red (cyan/blue) symbols denote data in the horizontal (vertical) plane. Note that greigite-dominated samples (SIRM/κ_{LF} >> 10 kAm^{-1}) in (d and f) had to be displayed with a significantly higher scaling, indicated by olive-colored axes in the diagrams and the scale bars. Red and blue symbols mark the AF demagnetization steps used for ChRM determination. AF demagnetization steps were 0, 5, 10, 15, 20, 30, 40, 50, 65, 80, and 100 mT. $_{\kappa LF}$: low-field magnetic susceptibility; SIRM: saturated iso-thermal remanent magnetization.

6 (Figure 3). Paleomagnetic data from core MSM33-55-1 (Liu et al., 2019) were too much affected by greigite for being included in the paleomagnetic stack. However, the core was important for correlation of MIS 6 sediments, using Ca/Ti and K/Ti log-ratios, since it is one of the few records extending from MIS 6 into MIS 5 (Figures 2, 3, and S1). Paleomagnetic data from cores MSM33-62-1 and MSM33-63-1 (Liu et al., 2018) from 146 ka back to 155 ka also had to be omitted because data from this interval was widely not correlatable, due to low sedimentation rates and/or short hiatuses of uncertain position. The final data collection of inclination, declination, and relative paleointensity records, together with the respective stacks, is shown in Figure 7. Directions were averaged in time bins of 200 years, using Fisher (1953) statistics. Therefore, error ranges for inclination and declination are given as α_{95} values. Relative paleointensities were also stacked into 200 year-bins with errors given as 1σ. Although the individual records cover different time intervals a fairly well constrained paleomagnetic record could be compiled from 130 ka back to about 170 ka, with a less well defined extension to 180 ka (fragmentary data from cores MSM33-56-1 and 57-1). Data from early MIS 5 could not be used due to "contamination" with greigite and other nonmagnetic sulfides, such as pyrite framboids. This new PSV record from MIS 6 comprises the data from 1,074 samples. The number of samples per time bin, stacked directions, relative paleointensities, and the PSV index are shown in Figure 8

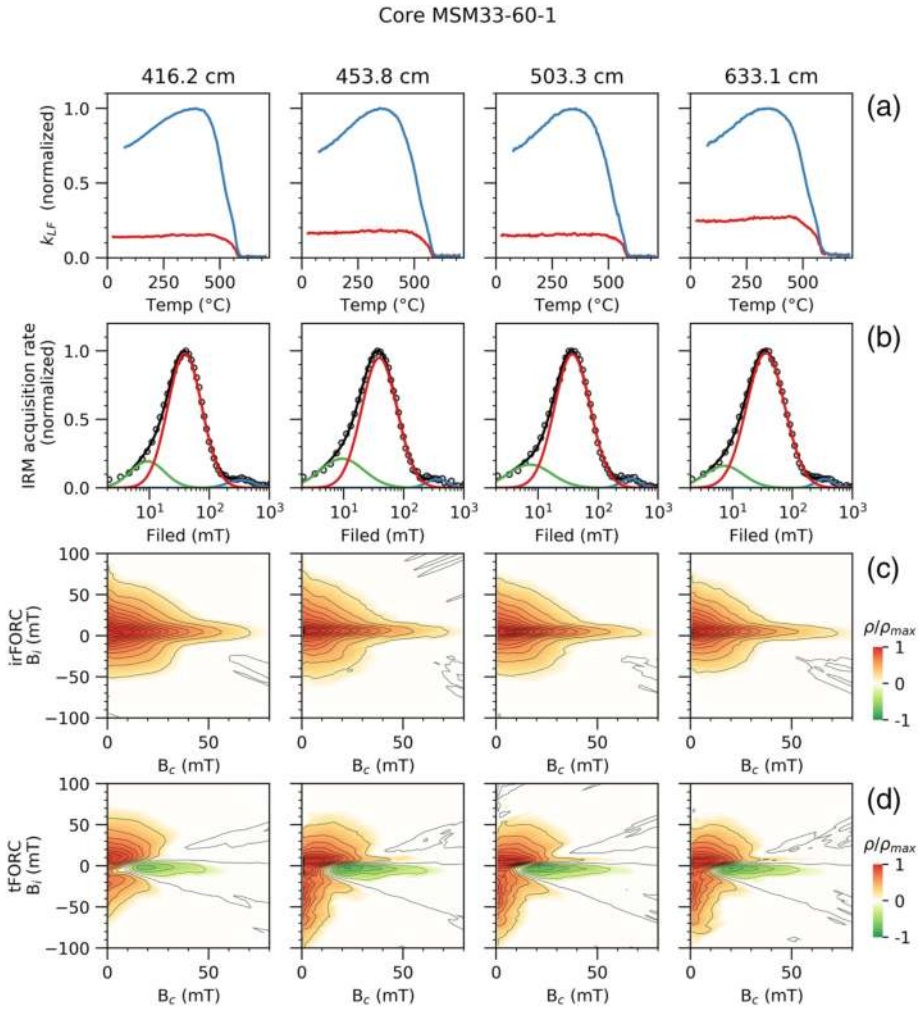

Figure 5. Rock magnetic results of four samples selected from core MSM33-60-1, representative for samples used for paleomagnetic stacking (SIRM/κ_{LF} < 10 kAm^{-1}). The corresponding demagnetization results are shown in Figure 4. (a) In high-temperature magnetic susceptibility κ_{LF} curves, red (blue) lines represent heating (cooling) curves. (b) In isothermal remanent magnetization (IRM) decomposition curves, circles indicate IRM acquisition rates determined from the gradient of IRM data. The green, red and blue lines denote three different components fitted to these data, whereas the black line is the fitted total spectrum. (c) irregular FORC (irFORC) and (d) transient hysteresis FORC (tFORC) diagrams were calculated with a smooth factor (SF) of 3 and their distributions ρ were normalized by their respective maximum ρ_{max}.

in the paleoenvironmental context of MIS 6 in the Black Sea, represented by XRF-derived element ratios of the sediments (K/Ti and Ca/Ti) and the $\delta^{18}O$ composite record, with the transition from lacustrine to marine water conditions at 127 ka.

4. Discussion

4.1. PSV During MIS 6 From Black Sea Sediments

While reconstructed lake surface temperature (LST) trends and oxygen isotopes are likely related to the long-lasting discharge of colder meltwater into the Black Sea "Lake" from the retreating Eurasian Ice Sheet (EIS), millennial-scale variability in LST and IRD proxy records clearly point to subdued Dansgaard-Oeschger (DO)-type cycles (Dansgaard et al., 1993), particularly during the first part of MIS 6. After ~160 ka BP, the Black Sea was more "locked" in a stable colder condition due to the expansion of

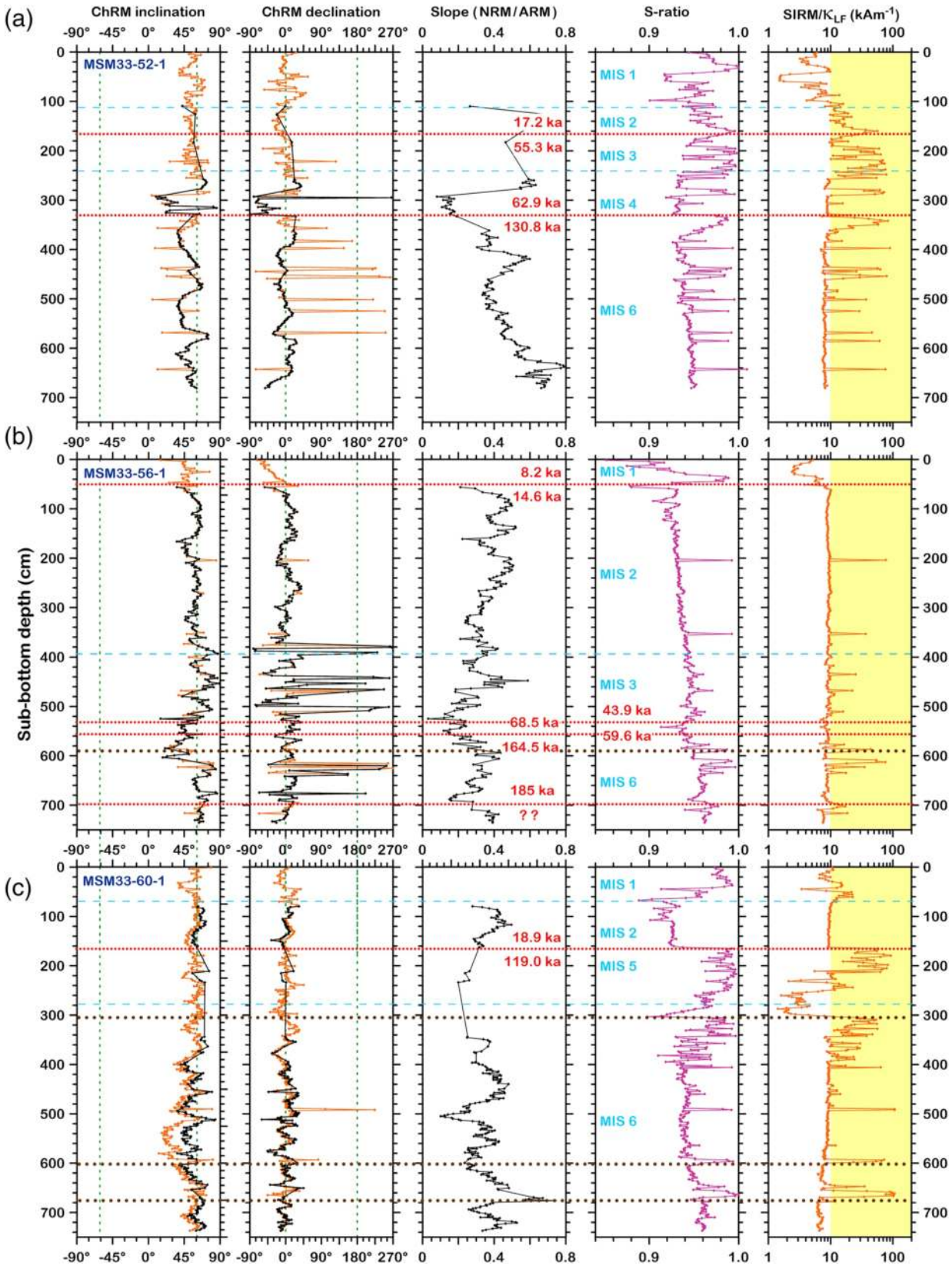

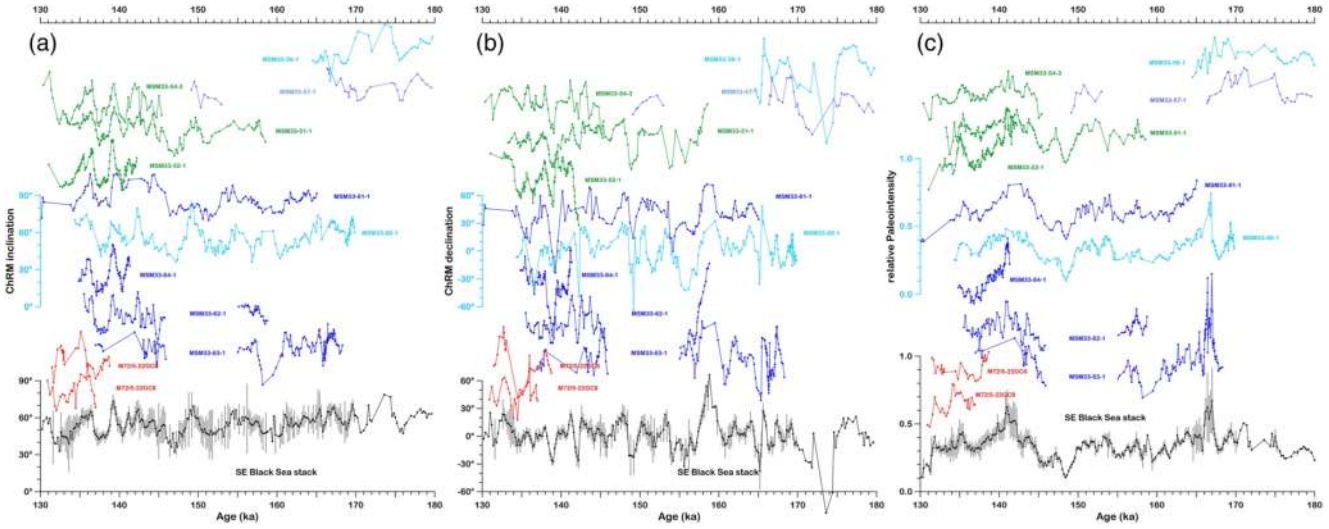

Figure 7. Paleomagnetic results from 12 Black Sea sediment cores for MIS 6 versus age: Individual and stacked records of (a) ChRM inclination and (b) declination, with error bars defined by the α_{95} from Fisher (1953) statistics used for stacking, and (c) relative paleointensity (slope (NRM/ARM)) with 1σ error bars. Data records are shown with a constant offset from core to core, with one *y*-axis each shown in the same color as the corresponding core and stacked data shown in black. Original data not presented in this study was previously published according to Table 1.

the EIS and the southward migration of the atmospheric polar front over the Black Sea region (Wegwerth et al., 2019, 2020). But, these climatic expression are less pronounced when compared to the sequence of DO-events from the last glacial (MIS 2-4; Nowaczyk et al., 2012). Therefore, correlation of the 12 cores used for stacking paleomagnetic data (Figure 7) was not straightforward. Element ratios show only subtle, nevertheless significant variations (Figures 8f and 8g) which are even not clearly related to the $\delta^{18}O$ record (Figure 8h). On the other hand, such fairly homogeneous sediments are ideal recorders of magnetic field variations, since concentration and grain size-related rock magnetic properties are also fairly homogeneous (Figure 6). The obtained PSV record is characterized by declination (inclination) oscillations of ±30° (±15°) about the expected dipole direction ($D = 0, I = 61°$), with periods of about 2000–4,000 years (Figures 8b and 8c). Since the stack does not reach back to MIS 7, the geomagnetic Iceland Basin excursion that occurred at the MIS 7/6 boundary (188 ka; see review by Channell et al., 2020) could not be found in the analyzed sediments. Relative paleointensities (Figure 8d) show a dynamic range of about 6:1 (intensities at 141.0 ka and 148.5 ka). The PSV index (Figure 8e) does not indicate any further excursional behavior (PSV index > 0.5) after the Iceland basin excursion in the studied Black sea sediments between 180 and 130 ka. Only twice the PSV index clearly exceeds 0.3 (but doesn't reach 0.5), indicating some enhanced PSV at ~159 ka (easterly declination swing) and ~148 ka (low intensity, low inclination). The westerly declinations (but with steep inclinations) at ~174 ka also exceed 0.3, but this feature is represented by only two samples, too sparsely constrained for an interpretation. Thus, in summary, the obtained MIS 6 Black Sea paleomagnetic record from 130 ka back to 180 ka represents mostly normal PSVs.

Figure 6. Paleo- and rock magnetic results from cores (a) MSM33-52-1, (b) MSM33-56-1, and (c) MSM33-60-1. ChRM inclinations and declination (left) are shown as raw results (orange) and as corrected data (black) after corrections for a titled magnetic fabric (see Section 3.2) and filtering out of greigite-affected samples with SIRM/κ_{LF} > 10 kAm^{-1}, marked in yellow (outer right). Data from Holocene and Eemian sapropelitic sediments were generally removed from the records due to their lithology being completely different from the glacial sediments. Slope (NRM/ARM) represents relative paleointensity variations (middle, only filtered data). S-ratio and SIRM/κ_{LF} represent magneto-mineralogical variations. Identified hiatuses are marked by horizontal red dotted lines, with their durations indicated by age ranges in red. Horizontal blue dashed lines indicate boundaries of marine isotope stages (MIS). Horizontal brown dotted lines indicate the position of identified tephra layers (Wegwerth at al., 2019). Vertical green dashed lines in the inclination and declination plots mark the direction of a geocentric axial dipole at the study site. ChRM-characteristic remanent magnetization, NRM (ARM)-natural (anhysteretic) remanent magnetization, S-ratio see Section 2.3, SIRM-saturated isothermal remanent magnetization, κ_{LF}-low-field magnetic susceptibility.

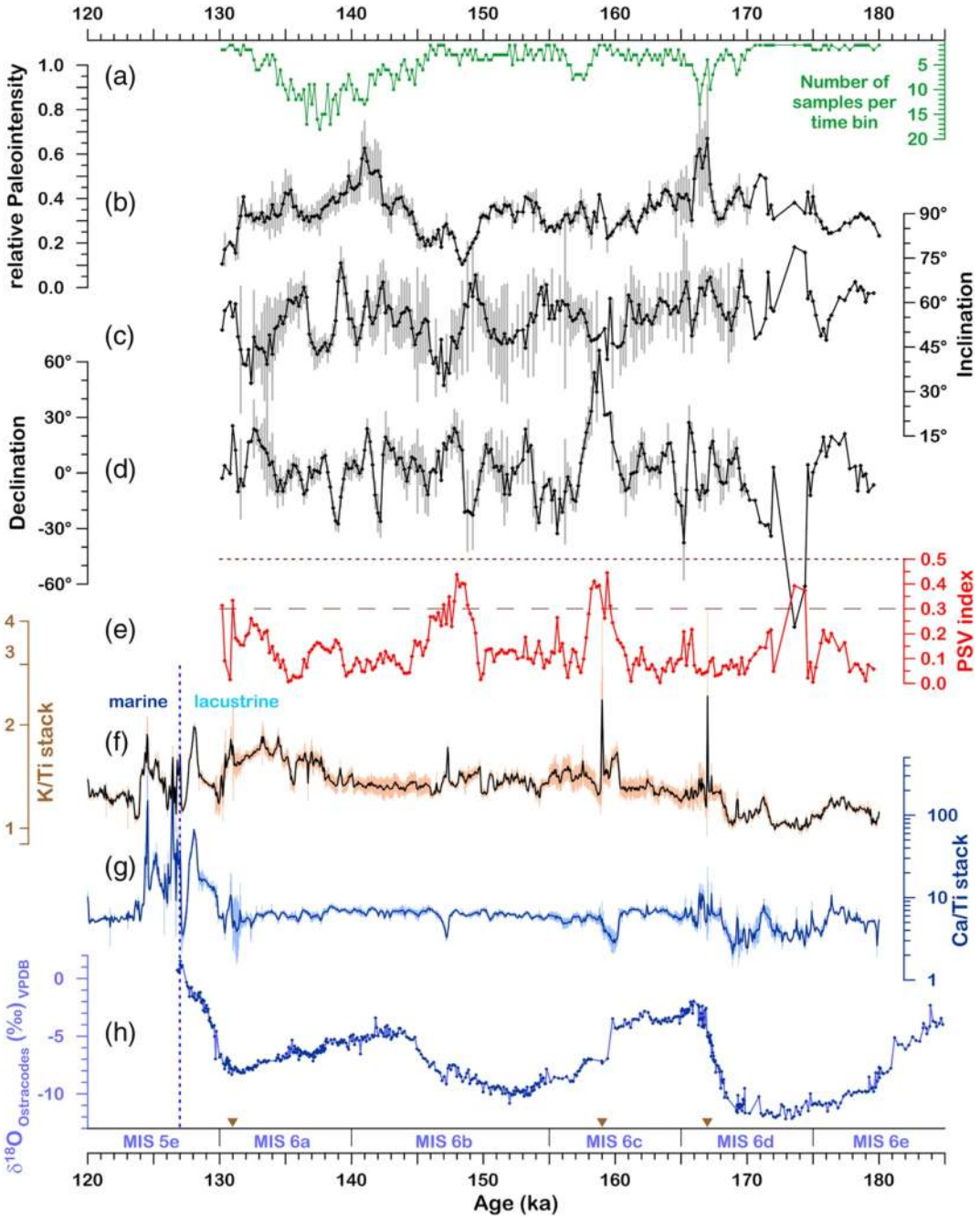

Figure 8. The Black Sea MIS 6 paleosecular variation record in its paleoclimatic context: (a) Number of samples per time bin (total number = 1,074), stacks of (b) relative paleointensity, (c) inclination and (d) declination, with error bars according to Figure 7, (e) the paleosecular variation (PSV) index (Panovska & Constable, 2017; Liu et al., 2020), together with stacks of XRF-derived element ratios of (f) K/Ti (comp. Figure S1) and (g) Ca/Ti (Figure 2), with 1 σ error bars, as well as (h) the $\delta^{18}O$ composite record from MIS 6 sediments (Wegwerth et al., 2019). Brown triangles in the bottom indicate the positions of three tephra layers. In (e) the horizontal dashed (dotted) line marks the threshold for normal secular variation (excursional behavior) with a PSV index ≤ 0.3 (PSV index > 0.5). The vertical blue dashed line in (f–h) indicates the transition from lacustrine to marine conditions in the Black Sea Basin in early MIS 5e.

4.2. Comparison to Other Paleomagnetic Records

A 149 m long core, reaching ~350 ka back in time, was recovered to the South of the Black Sea from Lake Van, Turkey, at ICDP (International Continental scientific Drilling Program) Site 5034-2. Due to the special

chemistry of the water body in the lake, magnetizations of the recovered sediments are fairly low. Therefore, paleomagnetic results published by Vigliotti et al. (2014) are quite noisy and a detailed comparison between Lake Van and Black Sea data is not possible.

An about 456 m long sediment composite profile, going back to ~1.3 Ma, has been created from four parallel cores from Lake Ohrid, Macedonia and Albania, at ICDP Site 5045 (Wagner et al., 2014), sited to the West of the Black Sea. The age model back to 637 ka is mainly based on tephrochronology and tuning of sedimentological parameters to orbital parameters (Francke et al., 2016). Further age constraints could be derived by some high-resolution magnetostratigraphic investigation on the Matuyama-Brunhes reversal and the Jaramillo subchron (Just et al., 2019) with discrete samples taken side by side, while the whole composite profile was generally sampled only every 50 cm. This was decided due to the fact that greigite frequently occurs in the sediments, as confirmed by rock magnetic investigations (Just et al., 2016). However, sediments in Lake Ohrid from 130 ka back to 180 ka (~MIS 6) are mostly free of greigite. MIS 6 sediments spread over about 30 m, thus yielding a total of about 60 samples, equal to one sample about every 830 years. Compared to the 225 tie points of the stacked Black Sea PSV record, this is a low-resolution record. At least, the overall pattern of the high-resolution Black Sea paleointensity and inclination records can be recognized in the Lake Ohrid paleomagnetic data, but details are lost due to the low resolution (Figure 9). However, due to a stratigraphic thickness of about 30 m, MIS 6 sediments at ICDP Site 5045 offer a high potential for future magnetostratigraphic investigations, probably confirming and better constraining the record of the Iceland Basin excursion, currently only supported by two samples (Figure 9b).

Long-term trends in inclination and a sharp inclination low around 150 ka in the Black Sea record also roughly correlate to another low-resolution record from Lake Yammoûneh, Lebanon (Develle et al., 2011), with a mean resolution of 1,000 years (Figure 9a). This is a further, though weak confirmation of the obtained directional data from a site relatively close to the study site in the Black Sea. Inclinations and tentative paleointensity estimates from MIS 6 sediments are also available from a 100 m core recovered from a paleolake in the Neualbenreuth Maar structure, SE Germany (Rohrmüller et al., 2018) far to the Northwest of the Black Sea. Inferred MIS 6 (Stebich et al., 2020) spreads over 35 m of sediments, but these are composed of coarse-grained silici-clastic deposits with numerous sand layers (likely turbidites), causing scattered directions and relative paleointensity data. In addition, greigite is found at many stratigraphic levels. Therefore, this record cannot serve as a reference for this study.

Paleointensity data of the global PISO1500 stack, mainly based on marine data from the North Atlantic with further data from the South Atlantic, the Indian Ocean, and the west Pacific, with a resolution of 1,000 years (Channell et al., 2009) show a quite good match with the corresponding Black Sea data (Figure 9g). Paleointensities collected only from the North Atlantic but stacked at a higher resolution of 500 years, the HINAPIS-1500 stack (Xuan et al., 2016) shows similar trends but differ from both the Black Sea data and the PISO1500 stack when looking into detail. Both the PISO1500 and HINAPIS-1500 stacks are linked to oxygen isotope stratigraphy. Thus, their age tie points are mostly defined by the MIS boundaries only. Compared with this, the Black Sea stack age model is based on numerous intra-MIS 6 age tie points, obtained from a detailed oxygen isotope stratigraphy correlated to U/Th-dated speleothem records from around the Black Sea (Wegwerth et al., 2019). Therefore, we think that the Black Sea paleomagnetic record is better constrained in age. In addition, it also comprises inclination and declination data, reproducibly recorded in up to 12 cores from nearby sites, making it the first high-resolution PSV record for MIS 6 for SE Europe/SW Asia.

Embedded in a comprehensive multidisciplinary investigation, this study now completes the paleo- and rock magnetic analyses performed on a total of 18 cores recovered during two ship expeditions to the Arkhangelsky Ridge, SE Black Sea. Together with data from the complementary studies on sediments from MIS 2 to 4, summarized by Liu et al. (2020), now a unique well-dated high-quality paleomagnetic data set, with temporal resolutions from 40 to 200 years, covering a total of one hundred thousand years of geomagnetic field activity, from normal secular variation to a short complete reversal of the geomagnetic field at 41 ka, is available. The time series from 14 to 68 ka and from 130 to 180 ka represent a profound data set needed for further analytical studies on a wider regional to global scale. Only in the scope of geomagnetic field models based on globally distributed paleomagnetic input data, such as the ones by, e.g., Korte et al. (2019) and Panovska et al. (2019), further insights into the dynamic evolution of the Earth's liquid outer core can

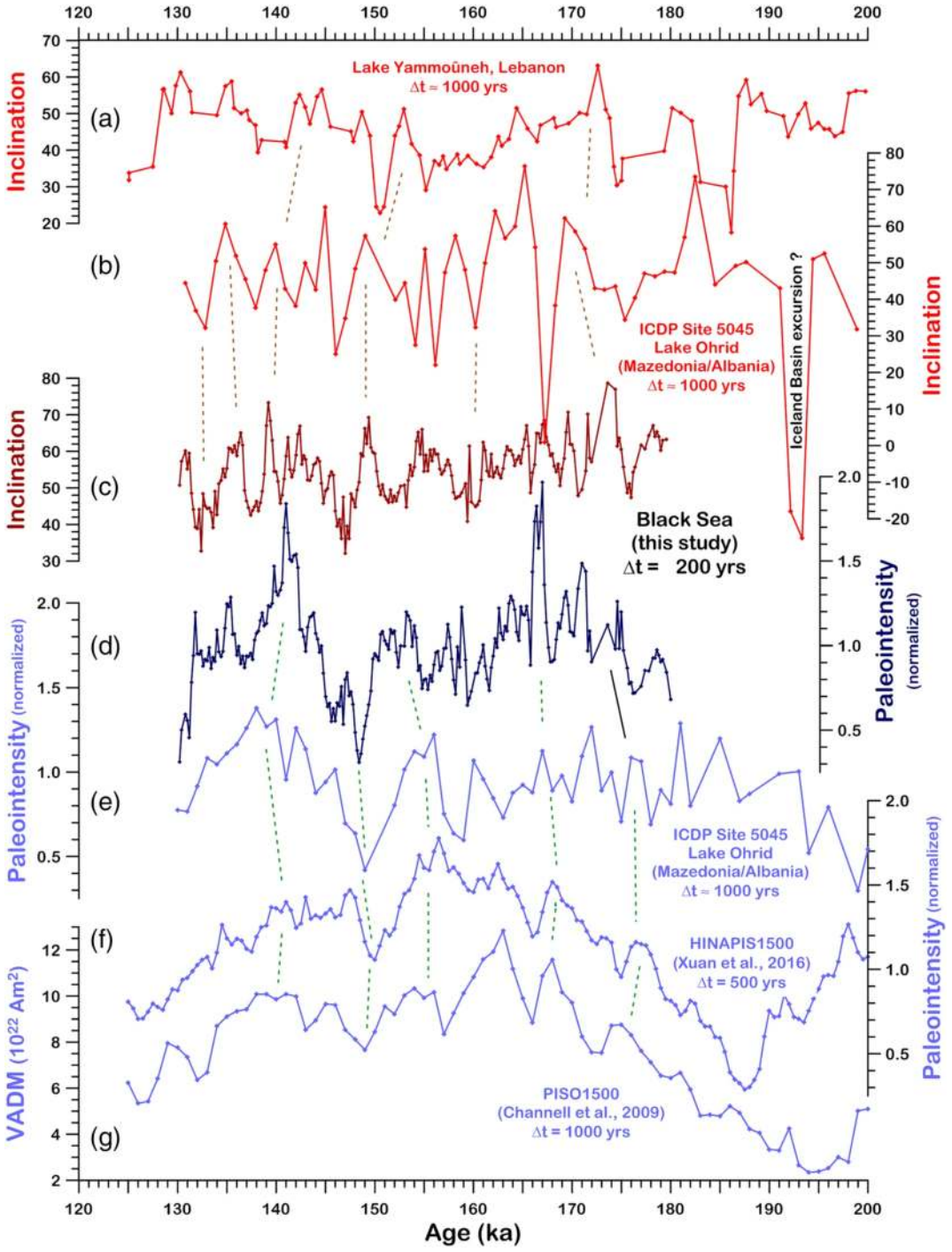

Figure 9. Inclination data and records of relative paleointensity from various sites compared to results from this study: inclinations from (a) Lake Yammoûneh, Lebanon (resampled from Develle et al., 2011), (b) Lake Ohrid, Macedonia and Albania (Just et al., 2016 & unpublished data), and (c) the Black Sea (this study), together with relative paleointensity from (d) the Black Sea (this study), (e) Lake Ohrid, Balkans (Just et al., 2016 & unpublished data), and (f) a stack of data from the North Atlantic (Xuan et al., 2016), and a record of the virtual axial dipole moment (VADM) derived from data of globally distributed sediment cores by Channell et al. (2009). Δt indicates the temporal resolution of data records shown here. Dashed lines trace possible correlatable features.

be gained. Thus, having a global view, the causes of temporal changes in direction and intensity of the geomagnetic field, from secular variation to reversals, can be much better understood.

5. Conclusions

Stacking of paleomagnetic data from a total of 12 sediment cores from the SE Black Sea yielded a high-quality composite PSV record including relative paleointensity covering most of MIS 6. Though individual partly fragmented records do not cover the whole time interval from 130 back to 180 ka, a well-dated and continuous high-resolution record could be compiled supported by correlation of high-resolution log-ratios (Ca/Ti, K/Ti) derived from XRF scanning and high-resolution records of magnetic susceptibility. Back to 170 ka the standard resolution is 200 years, with some gaps further back to 180 ka. The PSV index does not indicate any excursional features (PSV index > 0.5), only enhanced PSV could be found at ~159 ka (easterly declination) and ~148.5 ka (low intensity, low inclination), with 0.3 < PSV index < 0.5. Thus, the studied time span represents a fairly stable phase of the geomagnetic field. This new paleomagnetic record is an extension of the detailed reconstruction of geomagnetic field variations during MIS 2 to 4, also based on Black Sea sediments, published by Liu et al. (2020). In summary, the investigated MIS 6 glacial Black Sea sediments, deposited under oxic freshwater conditions, but now overlain by the world's largest anoxic waterbody, extended now one of the most detailed and best dated paleomagnetic MIS 2 to 4 records, available from the Northern hemisphere, to the penultimate glacial period.

Data Availability Statement

Oxygen isotope data presented in this study are available via: https://doi.org/10.1594/PANGAEA.906137. Stacked and individual paleomagnetic time series from the cores presented in this study are available via GFZ Data Services, Nowaczyk et al. (2021b), https://doi.org/10.5880/GFZ.4.3.2021.001. Standard rock magnetic data from all investigated cores taken during expedition M72/5 of German RV Meteor are available via GFZ Data Services, Nowaczyk et al. (2021c), https://doi.org/10.5880/GFZ.4.3.2021.002. Standard rock magnetic data from all investigated cores taken during expedition MSM33 of German RV Maria S. Merian are available via GFZ Data Services, Nowaczyk et al. (2021d), https://doi.org/10.5880/GFZ.4.3.2021.003.

Acknowledgments
We thank S. Plewe, M. Duwe, T. Moldenhawer, and F. Brendel for their technical and logistical help during processing and subsampling of the cores. We also thank the captains and crews of RV Meteor, cruise M72/5 and RV Maria S. Merian, cruise MSM33, for their efforts in providing optimal scientific working conditions. We would like to thank the Associate Editor of JGR-Solid Earth, Mark Dekkers, and two anonymous reviewers for their constructive comments. This work was partialy funded by the German Research Foundation (Deutsche Forschungsgemeinschaft, DFG SPP 1266 "INTERDYNAMIC" grants AR 367/9-1 and AR 367/9-2; WE 6136/1-1: BlackPearl), the Gary Comer Science and Education Foundation, U.S.A., and the Chinese Scholarship Council (CSC grant No. 201506180060). Open Access funding enabled and organized by Projekt DEAL.

References

Arz, H. W., Böttcher, M. E., Burmeister, C., Dellwig, O., Fisch, K., Hehl, U., et al. (2014). *Biological/Biogeochemical processes and element fluxes at the Black Sea pelagic redoxcline, sedimentation processes and the late Holocene development of the system* (pp. 63). Maria S. MERIAN-Berichte. Cruise No. MSM33, B.

Badertscher, S., Fleitmann, D., Cheng, H., Edwards, R. L., Gokturk, O. M., Zumbuhl, A., et al. (2011). Pleistocene water intrusions from the Mediterranean and Caspian seas into the Black Sea. *Nature Geoscience*, *4*, 236–239.

Channell, J. E. T., Singer, B. S., & Jicha, B. R. (2020). Timing of Quaternary geomagnetic reversals and excrusions in volcanic and sedimentary archives. *Quaternary Science Reviews*, *228*, 106114.

Channell, J. E. T., Xuan, C., & Hodell, D. A. (2009). Stacking paleointensity and oxygen isotope data for the last 1.5 Myr (PISO-1500). *Earth and Planetary Science Letters*, *283*(1–4), 14–23.

Cullen, V. L., Smith, V. C., & Arz, H. W. (2014). The detailed tephrostratigraphy of a core from the south-east Black Sea spanning the last ~60 ka. *Journal of Quaternary Science*, *29*(7), 675–690. https://doi.org/10.1002/jqs.2739

Czymzik, M., Nowaczyk, N. R., Dellwig, O., Wegwerth, A., Muscheler, R., Christl, M., & Arz, H. W. (2020). Lagged atmospheric circulation response in the Black Sea region to Greenland-Interstadial 10. *Proceedings of the National Academy of Sciences*, *117*(46), 28649–28654. https://doi.org/10.1073/pnas.2005520117

Dansgaard, W., Johnson, S. J., Clausen, H. B., Dahl-Jensen, D., Gundestrup, N. S., Hammer, C. U., et al. (1993). Evidence for general instability of past climate from a 250-kyr ice-core record. *Nature*, *364*, 218–220.

Demory, F., Nowaczyk, N. R., Witt, A., & Oberhänsli, H. (2005). High-resolution magnetostratigraphy of late quaternary sediments from lake Baikal, Siberia: Timing of intracontinental paleoclimate responses. *Global and Planetary Change*, *46*, 167–186.

Develle, A.-L., Gasse, F., Vidal, L., Williamson, D., Demory, F., Van Campo, E., , &(2011). A 250 ka sedimentary record from a small karstic lake in the Northern Levant (Yammoûneh, Lebanon) paleoclimatic implications. *Palaeogeography, Palaeoclimatology, Palaeoecology*, *305*, 10–27. https://doi.org/10.1016/j.palaeo.2011.02.008

Fisher, R. (1953). Dispersion on a sphere. *Proceedings of the Royal Society A: Mathematical, Physical and Engineering Sciences*, *217*(1130), 295–305. https://doi.org/10.1098/rspa.1953.0064

Francke, A., Wagner, B., Just, J., Leicher, N., Gromig, R., Baumgarten, H., et al. (2016). Sedimentological processes and environmental variability at Lake Ohrid (Macedonia, Albania) between 637 ka and the present. *Biogeosciences*, *13*, 1179–1196. https://doi.org/10.5194/bg-13-1179-2016

Heslop, D., McIntosh, G., & Dekkers, M. J. (2004). Using time- and temperature-dependent Preisach models to investigate the limitations of modelling isothermal remanent magnetization acquisition curves with cumulative log Gaussian functions. *Geophysical Journal International*, *157*, 55–63. https://doi.org/10.1111/j.1365-246X.2004.02155.x

Just, J., Nowaczyk, N. R., Sagnotti, L., Francke, A., Vogel, H., Lacay, J. H., & Wagner, B. (2016). Environmental control on the occurrence of high-coercivity magnetic minerals and formation of iron sulfides in a 640 ka sediment sequence from Lake Ohrid (Balkans). *Biogeosciences*, *13*, 2093–2109. https://doi.org/10.5194/bg-13-2093-2016

Just, J., Sagnotti, L., Nowaczyk, N. R., Francke, A., & Wagner, B. (2019). Recordings of fast paleomagnetic reversals in a 1.2 Ma greigite-rich sediment archive from Lake Ohrid, Balkans. *Journal of Geophysical Research: Solid Earth*, *124*. https://doi.org/10.1029/2019JB018297

Kirschvink, J. L. (1980). The least-squares line and plane and the analysis of palaeomagnetic data. *Geophysical Journal International*, *62*(3), 699–718. https://doi.org/10.1111/j.1365-246X.1980.tb02601.x

Koltai, G., Spötl, C., Shen, C. C., Wu, C. C., Rao, Z., Palcsu, L., et al. (2017). A penultimate glacial climate record from southern Hungary. *Journal of Quaternary Science*, *32*, 946–956.

Korte, M., Brown, M. C., Panovska, S., & Wardinski, I. (2019). Robust characteristics of the Laschamp and Mono Lake geomagnetic excursions: Results from global field models. *Frontiers of Earth Science*, *7*, 86. https://doi.org/10.3389/feart.2019.00086

Korte, M., & Constable, C. (2011). Improving geomagnetic field reconstructions for 0-3 ka. *Physics of the Earth and Planetary Interiors*, *188*, 247–259. https://doi.org/10.1016/j.pepi.2011.06.017

Korte, M., Constable, C., Donadini, F., & Holme, R. (2011). Reconstructing the Holocene geomagnetic field. *Earth and Planetary Science Letters*, *312*, 497–505. https://doi.org/10.1016/j.epsl.2011.10.031

Liu, J., Nowaczyk, N. R., Frank, U., & Arz, H. W. (2018). A 20–15 ka high-resolution paleomagnetic secular variation record from Black Sea sediments – no evidence for the 'Hilina Pali excursion'?. *Earth and Planetary Science Letters*, *492*, 174–185. https://doi.org/10.1016/j.epsl.2018.04.014

Liu, J., Nowaczyk, N. R., Frank, U., & Arz, H. W. (2019). Geomagnetic paleosecular variation record spanning from 40 to 20 ka – implications for the Mono Lake excursion from Black Sea sediments. *Earth and Planetary Science Letters*, *509*, 114–124. https://doi.org/10.1016/j.epsl.2018.12.029

Liu, J., Nowaczyk, N. R., Panovska, S., Korte, M., & Arz, H. (2020). The Norwegian-Greenland Sea, the Laschamps and the Mono Lake excursions recorded in a Black Sea sedimentary sequence spanning from 68.9 to 14.5 ka. *Journal of Geophysical Research*, *125*, e2019JB019225. https://doi.org/10.1029/2019JB019225

Lund, S. P. (2018). A new view of long-term geomagnetic field secular variation. *Frontiers of Earth Science*, *6*, 40. https://doi.org/10.3389/feart.2018.00040

Lund, S. P., Stoner, J. S., Channell, J. E. T., & Acton, G. (2006). A summary of Brunhes Chron paleomagnetic field variability recorded in Ocean Drilling Program cores. *Physics of the Earth and Planetary Interiors*, *156*, 194–204.

Nowaczyk, N. R. (2020). Redeposition experiments with natural sediments from the SE Black Sea in magnetic fields between about 2 and 114 μT. *Geophysical Journal International*, *484*, 15–29. https://doi.org/10.1093/gji/ggaa455

Nowaczyk, N. R., Arz, H. W. W., Frank, U., Kind, J., & Plessen, B. (2012). Dynamics of the Laschamp geomagnetic excursion from Black Sea sediments. *Earth and Planetary Science Letters*, *351–352*, 54–69. https://doi.org/10.1016/j.epsl.2012.06.050

Nowaczyk, N. R., Frank, U., Kind, J., & Arz, H. W. (2013). A high-resolution paleointensity stack of the past 14 to 68 ka from black sea sediments. *Earth and Planetary Science Letters*, *384*, 1–16. https://doi.org/10.1016/j.epsl.2013.09.028

Nowaczyk, N. R., Liu, J., & Arz, H. W. (2021a). Records of the Laschamps geomagnetic polarity excursion from Black Sea sediments: magnetite vs. greigite, discrete sample vs. U-channel data. *Geophysical Journal International*, *224*, 1079–1095. https://doi.org/10.1093/gji/ggaa506

Nowaczyk, N. R., Liu, J., & Arz, H. W. (2021b). *Paleosecular variation data for marine isotope stage 6 from SE Black Sea*. GFZ Data Services. https://doi.org/10.5880/GFZ.4.3.2021.001

Nowaczyk, N. R., Liu, J., & Arz, H. W. (2021c). *Rock magnetic data from sediments from the Arkhangelsky Ridge, SE Black Sea, I - cores from expedition M72/5, German RV Meteor, 2007*. GFZ Data Services. https://doi.org/10.5880/GFZ.4.3.2021.002

Nowaczyk, N. R., Liu, J., & Arz, H. W. (2021d). *Rock magnetic data from sediments from the Arkhangelsky Ridge, SE Black Sea, II - cores from expedition MSM33, German RV Maria S. Merian, 2013*. GFZ Data Services. https://doi.org/10.5880/GFZ.4.3.2021.003

Nowaczyk, N. R., Liu, J., Frank, U., & Arz, H. W. (2018). A high-resolution paleosecular variation record from Black Sea sediments indicating fast directional changes associated with low field intensities during marine isotope stage (MIS) 4. *Earth and Planetary Science Letters*, *484*, 15–29. https://doi.org/10.1016/j.epsl.2017.12.009

Panovska, S., & Constable, C. G. (2017). An activity index for geomagnetic paleosecular variation, excursions, and reversals. *Geochemistry, Geophysics, Geosystems*, *18*, 1366–1375. https://doi.org/10.1002/2016GC006668

Panovska, S., Korte, M., & Constable, C. G. (2019). One hundred thousand years of geomagnetic field evolution. *Reviews of Geophysics*, *57*, 1289–1337. https://doi.org/10.1029/2019RG000656

Roberts, A. P., Heslop, D., Zhao, X., & Pike, C. R. (2014). Understanding fine magnetic particle systems through use of first-order reversal curve diagrams. *Reviews of Geophysics*, *52*, 557–602. https://doi.org/10.1002/2014RG000462

Rohrmüller, J., Kämpf, H., Geiß, E., Großmann, J., Grun, I., Mingram, J., et al. (2018). Reconnaissance study of an inferred Quaternary maar structure in the western part of the Bohemian Massif near Neualbenreuth, NE-Bavaria (Germany). *International Journal of Earth Sciences*, *107*(4), 1381–1405. https://doi.org/10.1007/s00531-017-1543-0

Shumilovskikh, L. S., Arz, H. W., Wegwerth, A., Fleitmann, D., Marret, F., Nowaczyk, N., et al. (2013b). Vegetation and environmental changes in Northern Anatolia between 134 and 119 ka recorded in Black Sea sediments. *Quaternary Research*, *80*, 349–360.

Shumilovskikh, L. S., Fleitmann, D., Nowaczyk, N. R., Behling, H., Marret, F., Wegwerth, A., & Arz, H. W. (2014). Orbital- and millennial-scale environmental changes between 64 and 20 ka BP recorded in Black Sea sediments. *Climate of the Past*, *10*, 939–954.

Shumilovskikh, L. S., Marret, F., Fleitmann, D., Arz, H. W., Nowaczyk, N., & Behling, H. (2013a). Eemian and Holocene sea-surface conditions in the southern Black Sea: Organic-walled dinoflagellate cyst record from core 22-GC3. *Marine Micropaleontology*, *101*, 146–160.

Shumilovskikh, L. S., Tarasov, P., Arz, H. W., Fleitmann, D., Marret, F., Nowaczyk, N., et al. (2012). Vegetation and environmental dynamics in the southern Black Sea region since 18 kyr BP derived from the marine core 22-GC3. *Palaeogeography, Palaeoclimatology, Palaeoecology*, *337–338*, 177–193. https://doi.org/10.1016/j.palaeo.2012.04.015

Skinner, B. J., Erd, R. C., & Grimaldi, F. S. (1964). Greigite, the thio-spinel of iron; a new mineral. *American Mineralogist*, *49*, 543–555.

Stebich, M., Höfer, D., Mingram, J., Nowaczyk, N., Rohrmüller, J., Mrlina, J., & Kämpf, H. (2020). A contribution towards the palynostratigraphical classification of the Middle Pleistocene in Central Europe: The pollen record of the Neualbenreuth Maar, northeastern Bavaria (Germany). *Quaternary Science Reviews*, *250*, 106681. https://doi.org/10.1016/j.quascirev.2020.106681

Vigliotti, L., Channell, J. E. T., & Stockhecke, M. (2014). Paleomagnetism of Lake van sediments: chronology and paleoenvironment since 350 ka. *Quaternary Science Reviews*, *104*, 18–29. http://dx.doi.org/10.1016/j.quascirev.2014.09.028

Wagner, B., Wilke, T., Krastel, S., Zanchetta, G., Sulpizio, R., Reicherter, K., et al. (2014). The SCOPSCO drilling project recovers more than 1.2 million years of history from Lake Ohrid. *Scientific Drilling*, *17*, 19–29. https://doi.org/10.5194/sd-17-19-2014

Wegwerth, A., Dellwig, O., Kaiser, J., Ménot, G., Bard, E., Shumilovskikh, L., et al. (2014). Meltwater events and the Mediterranean reconnection at the Saalian–Eemian transition in the Black Sea. *Earth and Planetary Science Letters*, *404*, 124–135.

Wegwerth, A., Dellwig, O., Wulf, S., Plessen, B., Kleinhanns, I. C., Nowaczyk, N. R., et al. (2019). Major hydrological shifts in the Black Sea "Lake" in response to ice sheet collapses during MIS 6 (130–184 ka BP). *Quaternary Science Reviews*, *219*, 126–144. https://doi.org/10.1016/j.quascirev.2019.07.008

Wegwerth, A., Eckert, S., Dellwig, O., Schnetger, B., Severmann, S., Weyer, S., et al. (2018). Redox evolution during Eemian and Holocene sapropel formation in the Black Sea. *Palaeogeography, Palaeoclimatology, Palaeoecology*, *489*, 249–260.

Wegwerth, A., Ganopolski, A., Ménot, G., Kaiser, J., Dellwig, O., Bard, E., et al. (2015). Black Sea temperature response to glacial millennial-scale climate variability. *Geophysical Research Letters*, *42*, 2015GL065499.

Wegwerth, A., Kaiser, J., Dellwig, O., & Arz, H. W. (2020). Impact of Eurasian ice sheet and North Atlantic climate dynamics on Black Sea temperature variability during the penultimate glacial (MIS 6, 130–184 ka BP). *Paleoceanography and Paleoclimatology*, *35*, e2020PA003882. https://doi.org/10.1029/2020PA003882

Wegwerth, A., Kaiser, J., Dellwig, O., Shumilovskikh, L. S., Nowaczyk, N. R., & Arz, H. W. (2016). Northern hemisphere climate control on the environmental dynamics in the glacial Black Sea "Lake". *Quaternary Science Reviews*, *135*, 41–53.

Xuan, C., Channell, J. E. T., & Hodell, D. A. (2016). Quaternary magnetic and oxygen isotope stratigraphy in diatom-rich sediments from the Gardar Drift (IODP Site U1304, North Atlantic). *Quaternary Science Reviews*, *142*, 74–89. http://dx.doi.org/10.1016/j.quascirev.2016.04.010

Yamazaki, T., & Ioka, N. (1994). Long-term secular variation record of the geomagnetic field during the last 200 kyr recorded in sediment cores from the western equatorial Pacific. *Earth and Planetary Science Letters*, *128*, 527–544.

Yamazaki, T., Kanamatsu, T., Mizuno, S., Hokanishi, N., & Gaffar, E. Z. (2008). Geomagnetic field variations during the last 400 kyr in the western equatorial Pacific: Paleointensity-inclination correlation revisited. *Geophysical Research Letters*, *35*(20), L20307. https://doi.org/10.1029/2008GL035373

Yamazaki, T., & Yamamoto, Y. (2018). Relative paleointensity and inclination anomaly over the last 8 Myr obtained from the Integrated Ocean Drilling Program Site U1335 Sediments in the Eastern Equatorial Pacific. *Journal of Geophysical Research*, *B123*, 7305–7320. https://doi.org/10.1029/2018JB016209

Zhao, X., Roberts, A. P., Heslop, D., Paterson, G. A., Li, Y., & Li, J. (2017). Magnetic domain state diagnosis using hysteresis reversal curves. *Journal of Geophysical Research: Solid Earth*, *122*, 4767–4789. https://doi.org/10.1002/2016JB013683